INL/CON-23-72540-Revision-0

A Method of Estimating Sparse and Doubly-Dispersive Channels

October 2023

Brandon Hunt, David B. Haab, Behrouz Farhang-Boroujeny, Hussein Moradi

Changing the World's Energy Future

Idaho National Laboratory

INL is a U.S. Department of Energy National Laboratory operated by Battelle Energy Alliance, LLC

INL/CON-23-72540-Revision-0

A Method of Estimating Sparse and Doubly-Dispersive Channels

Brandon Hunt, David B. Haab, Behrouz Farhang-Boroujeny, Hussein Moradi

October 2023

Idaho National Laboratory
Idaho Falls, Idaho 83415

http://www.inl.gov

Prepared for the
U.S. Department of Energy
Under DOE Idaho Operations Office
Contract DE-AC07-05ID14517

A Method of Estimating Sparse and Doubly-Dispersive Channels

Brandon T. Hunt*, David B. Haab*, Hussein Moradi†, and Behrouz Farhang-Boroujeny*
*ECE Department, *The University of Utah*, brandon.t.hunt@utah.edu, david.haab@utah.edu, farhang@ece.utah.edu,
†Wireless Research Team, *Idaho National Laboratory*, hussein.moradi@inl.gov

***Abstract*—Using pilot-symbol assisted modulation, we develop a method to acquire channel information from signals received in low-SNR environments. First, we estimate the power-delay profile (PDP) of the channel. Then, we apply information from that estimate to obtain the channel coefficients only at points where the PDP is nonzero. Because we estimate a reduced number of channel coefficients, the complexity and estimation error are simultaneously reduced. We present a case study of the proposed estimation method when applied to a wideband skywave high frequency (HF) channel. Through this study, we find that the proposed approach has significantly enhanced performance when compared to an existing method that does incorporate sparsity information into its estimate. The improved low-SNR performance of the proposed estimator makes it particularly well suited for spread-spectrum and underlay waveforms.**

I. Introduction

In low signal-to-noise ratio (SNR) environments, channel estimates at the receiver become highly corrupted by noise which degrades system performance. In doubly-dispersive channels, this issue is compounded by the need to track or update the channel estimate over time, introducing even more noise into the channel estimates [1].

A key observation for many communications systems is that channels are often sparse in delay; that is, the channel impulse response has only a small number of nonzero coefficients relative to the total delay spread. An example of such a channel is the skywave high-frequency (HF) channel, where the impulse response may endure for several milliseconds but contains only a few significant paths [2]. By incorporating foreknowledge of sparsity into a channel estimator, the resulting error and complexity of the estimate can be reduced simultaneously [3].

Estimating sparse channels has been the topic of numerous studies. For instance, in [4]–[6], adaptive matching-pursuit based algorithms are developed and applied to estimating the doubly-dispersive channel responses of acoustic underwater channels. In [7] and [8], estimators are presented which assume the channel energy is concentrated at the beginning of the response, and so consider only a small number of taps spanning that region of time. The authors of [3] present a method referred to as 'most significant taps' where the channel is estimated for only those taps which are known to be nonzero. In [9], through the use of compressive sensing techniques, estimators which promote sparse solutions are shown to outperform traditional channel estimators, such as least-squares [10], using fewer training symbols.

However, despite these benefits, determining the positions of the nonzero taps requires the additional step of estimating the channel tap positions, several methods of which can be found in [11]–[13]. Unfortunately, estimating these nonzero tap positions at low SNRs using existing methods can lead to a large number of incorrectly-selected channel delays due to the magnitude of the noise.

Furthermore, in doubly-dispersive channels, the time-variation of the channel taps requires some tracking mechanism be employed by the receiver. A common tracking approach is to use decision feedback equalizers, such as those used in [1], [5], [14]; however, these remain prone to error propagation in low-SNR environments.

Hence, there is a need for a low-SNR channel estimator which can: 1), reliably estimate the nonzero-valued delays of a sparse channel response; and 2), effectively track the time-variation of the channel coefficients. To this end, in this work, we address these points by periodically inserting known pilot symbols into the data portion of the payload, a method referred to as pilot-symbol assisted modulation (PSAM) [15]. In doing so, we gain the ability to both determine the positions of nonzero channel taps as well as track their time variation at the expense of some reduction in spectral efficiency.

To develop the proposed estimator, we first estimate the channel power-delay profile (PDP) by exploiting positional knowledge of the inserted pilot symbols. From the estimated PDP, the nonzero channel taps are thus known and the channel estimate is obtained using only those nonzero-valued taps. Although the developed method is independent of the underlying modulation, we present results as it is applied to a filter-bank multicarrier spread-spectrum (FBMC-SS) communication system [16].

We note that the use of PDP information by a receiver to enhance data and channel recovery, particularly as it applies to OFDM, has been previously studied; e.g., [17]–[19]. However, the proposed approach in this work differs from these existing methods in three ways: first, the existing PDP estimators rely on exploiting the particular structure of multicarrier waveforms and do not generalize to single-carrier waveforms. Second, the

existing methods do not fully incorporate the prior information of the PDP in the channel estimate. Thirdly, and of greatest significance, the developed methods are neither applicable to low-SNR environments nor channels which admit lengthy delay spreads. The estimator that we propose herein is ambivalent to the underlying modulation, incorporates prior PDP information in the channel estimator, and demonstrates robust performance in both low-SNR and doubly-dispersive channel environments.

The remainder of this paper is organized as follows. In Section II, we begin with an overview of PSAM and the signal construction at the transmitter. The impact of the channel on the transmitted signal is also provided through relevant equations. In Section III, the proposed sparse channel estimation method is developed. In Section IV, we explore the proposed estimator through a case study as applied to HF sky-wave channels using FBMC-SS modulation [16]. Concluding remarks of the paper are made in Section V.

Notation: A combination of continuous-time, discrete-time, and vector notations are used in this paper with each denoted as $x(t)$, $x[n]$, and $\mathbf{x}$, respectively. Matrices are represented by bold uppercase letters, such as $\mathbf{X}$. $\mathbf{X}[l,k]$ is used to indicate the element at the l-th row and k-th column of $\mathbf{X}$. We also use the common notations $\mathbf{X}[l,:]$ and $\mathbf{X}[:,k]$ to refer to l-th row and k-th column of $\mathbf{X}$. Variables and parameters of functions are separated by a semicolon; e.g., $x(a;b)$ is a function of the input variable a and parameterized by b. The matrix $\boldsymbol{\mathcal{F}}$ is a DFT matrix that is normalized such that $\boldsymbol{\mathcal{F}}^{\mathrm{H}}\boldsymbol{\mathcal{F}} = \mathbf{I}$. We use the notation $\hat{x}$ to indicate an estimate of x. The convolution of two sequences is denoted by the symbol '$\star$'.

II. Pilot-Symbol Assisted Modulation

For each packet, we assume that the transmission begins with a periodic preamble sequence used for packet detection and channel training. This preamble is immediately followed by a mixed data/pilot symbol frame that we broadly refer to as the symbol frame; here, we provide some details of this section of the packet.

Consider a general transmitter setup where a mixed data-symbol and pilot-symbol vector $\mathbf{s}$ is given as

$$\mathbf{s} = [p_0, \underbrace{d_0, \ldots, d_{\lambda_\mathrm{p}-2}}_{\lambda_\mathrm{p}-1 \text{ elements}}, p_1, \underbrace{d_{\lambda_\mathrm{p}-1}, \ldots, d_{2\lambda_\mathrm{p}-2}}_{\lambda_\mathrm{p}-1 \text{ elements}}, \ldots]^{\mathrm{T}}, \quad (1)$$

where d_n is the n-th data symbol in the frame and p_k is the k-th pilot symbol. The pilot symbols are regularly placed every λ_p symbols in $\mathbf{s}$. In this work, we consider the pilot symbols to be complex-valued unity-magnitude scalars. Given a constant number of data symbols N_d, the total number of symbols N_s in the frame is

$$N_\mathrm{s} = \Big\lfloor \frac{\lambda_\mathrm{p} N_\mathrm{d}}{\lambda_\mathrm{p} - 1} \Big\rfloor, \quad (2)$$

where $\lfloor \cdot \rfloor$ denotes the floor operator.

To synthesize the transmitted signal, $\mathbf{s}$ is expanded and subsequently convolved with a pulse-shaping filter $g(t)$, yielding

$$\begin{aligned} x(t) &= \sum_{n=0}^{N_\mathrm{s}-1} s[n]\delta(t - nT_\mathrm{b}) \star g(t) \\ &= \sum_{n=0}^{N_\mathrm{s}-1} s[n] g(t - nT_\mathrm{b}), \end{aligned} \quad (3)$$

where T_b is the symbol interval.

The signal $x(t)$ is then transmitted through a time-varying channel $c(\tau;t)$. The signal contribution at the receiver input is thus

$$x_c(t) = \int_{-\infty}^{\infty} c(\tau;t) x(t-\tau) d\tau. \quad (4)$$

Correspondingly, the complete signal at the receiver input is given by $x_\mathrm{rx}(t) = x_c(t) + v(t)$, where $v(t)$ is a noise plus interference term. The received signal is then passed through the receiver matched filter $g^*(-t)$, yielding

$$\begin{aligned} y(t) &= g^*(-t) \star x_\mathrm{rx}(t) \\ &= \sum_{n=0}^{N_\mathrm{s}-1} s[n] \int_{-\infty}^{\infty} c(\tau;t)\eta(t - \tau - nT_\mathrm{b}) d\tau \\ &\qquad + g^*(-t) \star v(t), \end{aligned} \quad (5)$$

where $\eta(t) = g(t) \star g^*(-t)$.

Following [20], we express the channel response $c(\tau;t)$ as the sum of complex path gains at various delays, both of which may vary with time; i.e.,

$$c(\tau;t) = \sum_i c_i(t)\delta(\tau - \tau_i(t)), \quad (6)$$

where $c_i(t)$ and $\tau_i(t)$ represent the gain and delay of the i-th path, respectively.

Substituting (6) into (5) and rearranging gives

$$y(t) = \sum_i x_i(t) + \tilde{v}(t), \quad (7)$$

where $\tilde{v}(t) = g^*(-t) \star v(t)$ is a colored noise plus interference term and $x_i(t)$ is the component of $x_c(t)$ associated with the i-th channel path; specifically,

$$x_i(t) = c_i(t) \sum_{n=0}^{N_\mathrm{s}-1} s[n]\eta(t - \tau_i(t) - nT_\mathrm{b}). \quad (8)$$

The channel estimation and tracking method proposed in the following section uses a sampled version of the signal $y(t)$. We obtain the sampled, discrete-time signal $y[m]$ by sampling $y(t)$ at the rate $f_\mathrm{s} = Lf_\mathrm{b}$; equivalently, $y[m] = y(t)|_{t=mT_\mathrm{b}/L}$. We use '$m$' to denote the sample index, distinguishing it from the symbol index 'n'.

To present a sampled version of $x_i(t)$, we quantize the path delays $\tau_i(t)$ to some integer values denoted by m_i. We also remove their possible variation with time to simplify the following equations. With this assumption, the discrete time versions of (7) and (8) are

$$y[m] = \sum_i x_i[m] + \tilde{v}[m], \quad (9)$$

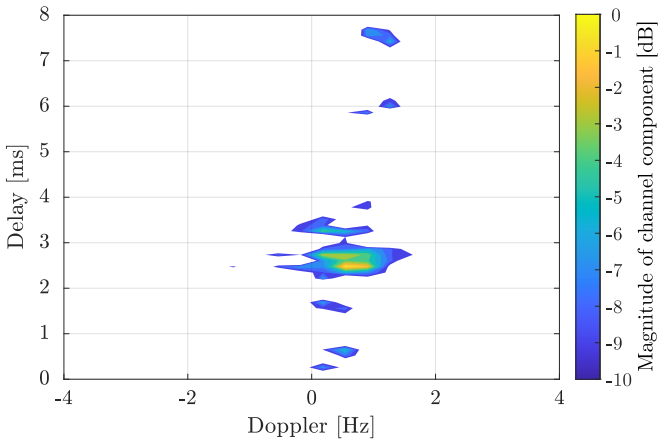

Fig. 1. A channel scattering plot measured between Idaho Falls, Idaho, in the United States and Sydney, Australia. We show only the channel components that are within 10 dB of the peak value.

where $\tilde{v}[m] = \tilde{v}(t)|_{t=mT_\mathrm{b}/L}$, and

$$x_i[m] = c_i[m] \sum_{n=0}^{N_\mathrm{s}-1} s[n]\eta[m - m_i - nL]. \tag{10}$$

Removing the time variation of the path delays m_i is justified if we assume that the path delays appear in time-contiguous clusters, such as those in skywave HF channels [2].

III. Channel Estimation

The channel estimator that we propose consists of two estimation stages: the first stage estimates the positions of the nonzero channel taps, and the second stage estimates the channel at those nonzero positions. To this end, in the first stage, we estimate the PDP of the channel. Then, in the second stage, we use the estimated PDP to modify a minimum mean-squared error (MMSE) channel estimator so that only the nonzero-valued channel paths are estimated.

A. PDP Estimator

To estimate the PDP of the channel, we first note that doubly-dispersive channels are statistically characterized by their scattering plots [21]. An example of a scattering plot that we measured over a skywave HF link between Idaho Falls, USA and Sydney, Australia is presented in Fig. 1. This plot reflects both the time dispersion (along the delay axis) and the time variation (along the Doppler axis) of the channel. Correspondingly, the PDP of the channel impulse response may be obtained by integrating the signal energy along the Doppler dimension for each value of delay [21]. Here, we develop a PDP estimation procedure that follows this methodology using the inserted pilot symbols in the symbol frame.

We assume that at the present stage of the receiver processing, the data packet has been detected and buffered in full. We thus have access to all the samples of $y[m]$ that carry the pilot symbols. To begin, we form a set of vectors $\mathbf{y}_k$, each of length M, centered around each of the pilot symbols. The indices of the pilot symbols within the vector $y[m]$ can be determined from the initial timing phase. The number of samples M in $\mathbf{y}_k$ should be chosen to contain the entire duration of the channel response from each respective pilot.

Next, given that there are a total of N_p pilot symbols, we organize the vectors into the M-by-N_p matrix

$$\mathbf{Y} = \left[\mathbf{y}_0\ \mathbf{y}_1\ \cdots\ \mathbf{y}_{N_\mathrm{p}-1}\right]. \tag{11}$$

From $\mathbf{Y}$, we generate a delay-time representation of the channel impulse response that we will then use to estimate the scattering function of the channel. To this end, we begin by forming the matrix

$$\hat{\mathbf{C}}_\eta = \mathbf{Y}\mathbf{P}^*, \tag{12}$$

where $\mathbf{P}$ is the diagonal matrix with elements p_0, p_1, $\cdots$, $p_{N_\mathrm{p}-1}$, and superscript '$*$' indicates conjugation. Note that this leads to

$$\hat{\mathbf{C}}_\eta[:,k] = p_k^* \mathbf{y}_k. \tag{13}$$

Next, we define a compound row-column index as $m_{lk} = l + k\lambda_\mathrm{p}L$. Combining (13) with (9) and (10), we find that

$$\hat{\mathbf{C}}_\eta[l,k] = \sum_i c_i[m_{lk}] \sum_{n=0}^{N_\mathrm{s}-1} p_k^* s[n]\eta[m_{lk} - m_i - nL] + \tilde{v}[m_{lk}]. \tag{14}$$

In (14), the symbol index where $n = k\lambda_\mathrm{p}$ coincides with the k-th pilot symbol. Then, recalling that $p_k^* p_k = 1$, (14) may be rearranged as

$$\begin{aligned}\hat{\mathbf{C}}_\eta[l,k] = &\sum_i c_i[m_{lk}]\eta[m_{lk} - m_i] \\ &+ \sum_i c_i[m_{lk}] \sum_{n\neq k\lambda_\mathrm{p}} p_k^* s[n]\eta[m_{lk} - m_i - nL] \\ &+ \tilde{v}[m_{lk}].\end{aligned} \tag{15}$$

In (15), the first summation contains the channel impulse response convolved with $\eta[m]$ and the second summation is interference introduced by the adjacent data symbols.

Next, we take the DFT along each row of $\hat{\mathbf{C}}_\eta$ and then square the magnitude of the result. This leads to the scattering function $\hat{\boldsymbol{\mathcal{S}}}_\eta$, [22], whose kl-th element is expressed as

$$\hat{\boldsymbol{\mathcal{S}}}_\eta[l,k] = \sum_i |\eta[m_{lk} - m_i]|^2 \Phi_{c_i c_i}[l,k] + \Phi_{\zeta\zeta}[l,k]. \tag{16}$$

Here, $\Phi_{c_i c_i}[l,k]$, $k = 0, 1, \cdots, N_\mathrm{p} - 1$ represents the power spectral density of the time-varying path gain sequence $c_i[m_{l0}]$, $c_i[m_{l1}]$, $\cdots$, which is equivalently the Doppler spread of the i-th path gain. Similarly, $\Phi_{\zeta\zeta}[l,k]$ contains the contributions arising from inter-symbol interference (ISI) and noise.

We can obtain the PDP by summing across the rows of the scattering function $\hat{\boldsymbol{\mathcal{S}}}_\eta$; however, the result will be adversely affected by the ISI plus noise term $\Phi_{\zeta\zeta}$. To minimize the impact of ISI and noise on the estimate, we take advantage of the fact that the Doppler spread $\Phi_{c_i c_i}$ occupies a limited range of frequencies. That is, the Doppler spread is significant only over a small region in $\hat{\boldsymbol{\mathcal{S}}}_\eta$. Considering this point, we instead obtain the PDP $\hat{\boldsymbol{\rho}}_\eta$ using a weighted sum as

$$\hat{\boldsymbol{\rho}}_\eta[l] = \sum_k w_k \hat{\boldsymbol{\mathcal{S}}}_\eta[l,k], \tag{17}$$

where w_k are the elements of $\mathbf{w}$, and $\mathbf{w}$ is a weighting vector that covers the Doppler range of the channel; in effect, $\mathbf{w}$ correlates with the band-limited Doppler spectrum.

Next, from (16) we observe that $\hat{\boldsymbol{\rho}}_\eta$ contains the channel PDP filtered by $|\eta[m]|^2$. Hence, using $\boldsymbol{\rho}_c$ to denote the underlying PDP of the channel, we can express $\hat{\boldsymbol{\rho}}_\eta$ as

$$\hat{\boldsymbol{\rho}}_\eta = \mathbf{N}\boldsymbol{\rho}_c + \bar{\boldsymbol{\zeta}}, \tag{18}$$

where $\mathbf{N}$ is a square circulant matrix that implements convolution with $|\eta[m]|^2$, and $\bar{\boldsymbol{\zeta}}$ is the ISI and noise term after the weighted summation along the Doppler dimension.

When the channel is sparse in the delay dimension, the estimation error is reduced by using ℓ_1-norm optimization methods which promote sparse solutions [23]. We thus formulate the following optimization:

$$\hat{\boldsymbol{\rho}}_c = \underset{\hat{\boldsymbol{\rho}}_c}{\arg\min} ||\hat{\boldsymbol{\rho}}_c||_{\ell_1} \quad \text{s.t.} \quad ||\hat{\boldsymbol{\rho}}_\eta - \mathbf{N}\hat{\boldsymbol{\rho}}_c||_{\ell_2} < \varepsilon. \tag{19}$$

This optimization is termed basis pursuit [23] and can be solved using a number of different algorithms; e.g., matching pursuit and its extensions [4], [24], [25]. In this work, we use the orthogonal matching pursuit (OMP) algorithm [24].

B. Channel Estimator

As discussed in Section II, the transmitted packet begins with a preamble that is used for both packet detection as well as a few initialization steps such as timing acquisition and equalization. In the previous subsection, we used the acquired timing phase and inserted pilots to identify the nonzero-valued delay taps in the channel response. Here, we first apply this nonzero-tap information to get a channel estimate from the received preamble sequence. This estimate is used to initialize the equalizer. We then describe how the inserted pilot symbols may be used to modify the equalizer weights and enable reliable channel tracking.

We assume that the preamble consists of a few cycles of a periodic signal containing Z symbols per cycle, and we assume the channel response has a negligible variation over each cycle. For such a preamble structure, following [26], we may express the r-th period of the received cyclic preamble as

$$\mathbf{y}_{\text{pre},r} = \mathbf{G}^{\text{H}}\mathbf{G}\mathbf{Z}\mathbf{c} + \mathbf{G}^{\text{H}}\mathbf{v}, \tag{20}$$

where $\mathbf{G}$ is a ZL-by-ZL circulant matrix that implements circular convolution with the filter $g[m]$. Similarly, the matrix $\mathbf{Z}$ is a circulant matrix constructed from a single period of the cyclic preamble symbols that have been expanded by L.

Next, from [27], any circulant matrix $\mathbf{A}$ can be factored as

$$\mathbf{A} = \boldsymbol{\mathcal{F}}^{\text{H}}\mathbf{A}_{\text{f}}\boldsymbol{\mathcal{F}}, \tag{21}$$

where $\mathbf{A}_{\text{f}}$ is a diagonal matrix whose elements are the DFT of the first column of $\mathbf{A}$. Applying (21) to (20) and incorporating knowledge of the nonzero tap positions, we can express $\mathbf{y}_{\text{pre},r}$ as

$$\mathbf{y}_{\text{pre},r} = \boldsymbol{\mathcal{F}}^{\text{H}}\mathbf{G}_{\text{f}}^{*}\mathbf{G}_{\text{f}}\mathbf{Z}_{\text{f}}\boldsymbol{\mathcal{F}}_{\text{p}}\mathbf{c}_{\text{p}} + \mathbf{G}^{\text{H}}\mathbf{v}, \tag{22}$$

where $\mathbf{c}_{\text{p}}$ is a pruned version of $\mathbf{c}$ containing only the nonzero taps of the channel, and similarly, $\boldsymbol{\mathcal{F}}_{\text{p}}$ is obtained by selecting the columns of $\boldsymbol{\mathcal{F}}$ corresponding to $\mathbf{c}_{\text{p}}$ [3].

From (22), the minimum mean squared error (MMSE) estimate of $\mathbf{c}_{\text{p}}$, [10], is obtained as

$$\hat{\mathbf{c}}_{\text{p}} = (\hat{\boldsymbol{\Sigma}}_{c_{\text{p}}c_{\text{p}}}^{-1} + \mathbf{D}_{\text{f}}^{\text{H}}\boldsymbol{\Sigma}_{\tilde{v}_{\text{f}}\tilde{v}_{\text{f}}}^{-1}\mathbf{D}_{\text{f}})^{-1}\mathbf{D}_{\text{f}}^{\text{H}}\boldsymbol{\Sigma}_{\tilde{v}_{\text{f}}\tilde{v}_{\text{f}}}^{-1}\boldsymbol{\mathcal{F}}\mathbf{y}_{\text{pre},r}, \tag{23}$$

where $\hat{\boldsymbol{\Sigma}}_{c_{\text{p}}c_{\text{p}}}$ and $\boldsymbol{\Sigma}_{\tilde{v}_{\text{f}}\tilde{v}_{\text{f}}}$ are the covariance matrices of $\mathbf{c}_{\text{p}}$ and $\tilde{\mathbf{v}}_{\text{f}} = \boldsymbol{\mathcal{F}}\mathbf{G}^{\text{H}}\mathbf{v}$, respectively, and

$$\mathbf{D}_{\text{f}} = \mathbf{G}_{\text{f}}^{*}\mathbf{G}_{\text{f}}\mathbf{Z}_{\text{f}}\boldsymbol{\mathcal{F}}_{\text{p}}. \tag{24}$$

The matrix $\hat{\boldsymbol{\Sigma}}_{c_{\text{p}}c_{\text{p}}}$ is a matrix which provides information about the prior probability of $\mathbf{c}_{\text{p}}$ [10]. Assuming the channel has uncorrelated scattering, $\hat{\boldsymbol{\Sigma}}_{c_{\text{p}}c_{\text{p}}}$ is a diagonal matrix whose entries are the estimated PDP, $\hat{\boldsymbol{\rho}}_c$.

The equalizer weights can be initialized by applying the estimator in (23) to the received preamble. To ensure these weights do not become outdated, we use the known pilot symbols to update the channel, and accordingly the equalizer, as we traverse the payload. To this end, we assume the inserted pilots are periodic with a period of Z symbols in $\mathbf{s}$. We construct a circulant matrix, $\mathbf{P}_{\text{e}}^{(k)}$, whose size is ZL-by-ZL and corresponds to the k-th pilot symbol. This matrix is formed in the same manner as $\mathbf{Z}$, except here, the pilot symbols are separated by $\lambda_{\text{p}}L - 1$ zeroes. Additionally, the vector $\mathbf{y}_{\text{pre},r}$ is replaced with the associated samples from $y[m]$ corresponding to the k-th pilot. Making the necessary replacements, (23) is then used to obtain the corresponding MMSE estimate of the channel from each pilot symbol.

We take the final step of denoising the channel estimates along the time axis by convolving them with a filter whose passband matches the expected Doppler spread of the channel. Note that at this stage, the Doppler spread of the channel is available from the estimate $\hat{\boldsymbol{\mathcal{S}}}_\eta$. We then interpolate the estimates to obtain the channel response for each data symbol within the symbol frame.

C. Complexity discussion

Here, we consider the complexity of the developed two-stage system, beginning with the PDP estimator. The PDP is estimated by the following five steps:

1) Obtain $\hat{\mathbf{C}}_\eta = \mathbf{Y}\mathbf{P}^*$. This step takes MN_{p}^2 complex multiplications and MN_{p}^2 complex additions.
2) Take the FFT of each row in $\hat{\mathbf{C}}_\eta$; this comprises M total N_{p}-point FFT operations.
3) Obtain the real-valued matrix $\hat{\boldsymbol{\mathcal{S}}}_\eta$ by squaring each element from the resulting matrix in step 2; this requires MN_{p} complex multiplications and 0 additions.
4) Obtain $\hat{\boldsymbol{\rho}}_\eta$ by performing a weighted sum across $\hat{\boldsymbol{\mathcal{S}}}_\eta$; this step requires MN_{p} real multiplications and MN_{p} real additions.
5) Estimate $\hat{\boldsymbol{\rho}}_c$ from $\hat{\boldsymbol{\rho}}_\eta$ using the OMP algorithm. Because the algorithm performs a variable number of loops that depends on the channel sparsity, we use the asymptotic behavior of this function. Using an efficient implementation of OMP [28], this algorithm has a complexity of $O\left(ZL(1+i)\right)$ per iteration, where i is the iteration number and the algorithm terminates after I iterations.

When the number of samples in the preamble is much greater than the number of pilot symbols, i.e., $ZL \gg N_{\text{p}}$, the

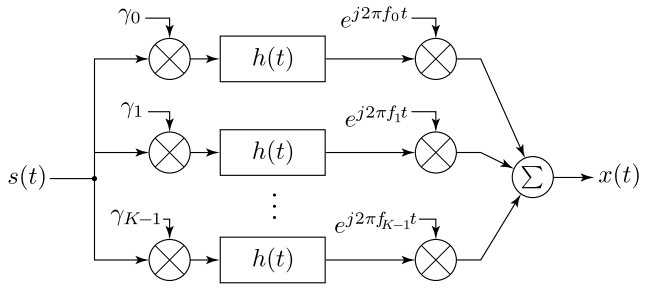

Fig. 2. The FBMC-SS transmitter structure. The input symbol stream $s(t)$ is spread across each of the parallel branches. Along each branch, the signal copy is phase-shifted by γ_k, filtered by $h(t)$, and translated to the respective subcarrier frequency.

complexity of the PDP estimator is dominated by the OMP algorithm.

Considering the channel-estimation stage defined in (23), the complexity is dominated by the matrix inversion which has complexity $O(\dim(\hat{\mathbf{c}}_\mathrm{p})^3)$, where $\dim(\cdot)$ denotes the number of elements in $\hat{\mathbf{c}}_\mathrm{p}$. This inversion must be performed once for every preamble sequence as well as for each of the N_p pilot symbols. Note that, when the channel vector is not pruned (i.e., $\mathbf{c}_\mathrm{p} = \mathbf{c}$), this operation has complexity $O((ZL)^3)$.

Hence, although estimating the PDP adds complexity to the system, it significantly reduces the dimensionality of the channel estimate $\hat{\mathbf{c}}_\mathrm{p}$. Because the overall complexity of the proposed two-stage approach will be asymptotically dominated by the length of the channel estimate vector, we argue that the additional computational burden incurred by estimating the channel PDP beforehand will be redeemed by the computational savings observed in the channel estimation stage.

IV. A Case Study: Results with FBMC-SS Modulation Over a Skywave HF Channel

To evaluate the performance of the developed two-stage channel estimation technique, we examine its performance as applied to a filter-bank multicarrier spread-spectrum (FBMC-SS) waveform in HF channels. We use the FBMC-SS waveform for its demonstrated robust performance at low-SNRs; e.g., [29], [30]. Similarly, we study the performance in HF channels because they are both doubly-dispersive and sparse in delay [2], and therefore pair well with the proposed channel estimation technique. Here, we provide a brief overview of the FBMC-SS waveform for completeness; see [16], [26], [30] for further details.

FBMC-SS is a multicarrier waveform in which data symbols are spread over K non-overlapping subcarriers. Fig. 2 provides a block diagram of the transmitter structure. The prototype filter $h(t)$ is a square-root raised cosine filter with a rolloff factor of $\alpha = 1$. The subcarrier frequencies are denoted by f_k and are spaced by $(1+\alpha)f_\mathrm{b}$ Hz. The γ_k coefficients are complex, unity-magnitude scalars that phase-shift each branch to reduce the PAPR of the synthesized waveform [30].

The transmit filter structure can be compactly represented as

$$g(t) = \frac{1}{\sqrt{K}}\, h(t) \sum_{k=0}^{K-1} \gamma_k e^{j2\pi f_k t}. \tag{25}$$

When the FBMC-SS waveform is constructed with the selection of rolloff factor $\alpha = 1$ and frequency spacing $(1+\alpha)f_\mathrm{b}$ Hz, from [16] it is found that

$$\eta(t) = \begin{cases} -0.5 & \text{for } t = \pm T_\mathrm{b}/2 \\ 1 & \text{for } t = 0 \\ 0 & \text{else.} \end{cases} \tag{26}$$

For the results presented here, we use an FBMC-SS waveform with $K = 32$ subcarriers at a symbol rate of $f_\mathrm{b} = 1000$ sym/s, leading to a sampling rate of $f_\mathrm{s} = 64000$ samples/s. We let $\lambda_\mathrm{p} = 8$, and each symbol frame has $N_\mathrm{d} = 448$ data symbols. Each preamble period contains $Z = 16$ symbols, and the pilot symbol sequence is periodic with a period of 2 pilots. Data encoding is performed using orthogonal multicodes [31]. The delay search range of the receiver spans 10 ms, leading to $M = 641$ samples. The weighting vector $\mathbf{w}$ is a Gaussian shape tuned for a Doppler width of 10 Hz; that is, the 2σ width of $\mathbf{w}$ extends from -10 to $+10$ Hz.

We test the channel estimator in a simulated HF channel following the form described in [32]. The simulated channel has two equal-power modes separated in time by 2 ms. Following [32] and [2], the PDP of each mode follows a Gamma distribution and each path fades with a Gaussian Doppler spectrum. The RMS delay spread of each mode is 80 μs and each path fades with a Doppler spread of 4 Hz (equivalently, a 2σ-width of 8 Hz).

A. PDP Estimator

We begin by considering the performance of the PDP estimator in isolation. For illustrative purposes, in Fig. 3, the PDP estimate obtained using (19) is compared to the actual PDP for only a single channel realization. The OMP algorithm terminated when the magnitude of the next tap estimate fell below 20% of the largest estimated tap magnitude. In this case, the algorithm terminated after estimating 12 PDP values.

Although the weighting vector $\mathbf{w}$ was set for a Doppler spread of 10 Hz and the channel faded at a rate of only 4 Hz, the dominant nonzero tap-values of the PDP were still recovered. This result suggests that exactly matching $\mathbf{w}$ to the Doppler spread of the channel is not critical.

We note that the termination threshold value as well as the Doppler window range must be specified *a priori*, and that, in practice, the optimal values for these quantities may be difficult to obtain. For this reason, here, our receiver uses the predetermined values of 20% for a threshold and a Doppler-profile width of 10 Hz. We note that pre-selecting certain values for practical implementations is a method adopted when estimating the parameters would be otherwise functionally prohibitive; e.g., in OFDM, where a certain length of CP is assumed to ensure ISI-free communication [19]. In our case, the chosen values provide enhanced performance across a variety of channel conditions despite being poorly matched to the actual parameters of the realized channel (specifically, when the channel Doppler spread is much narrower than the anticipated Doppler).

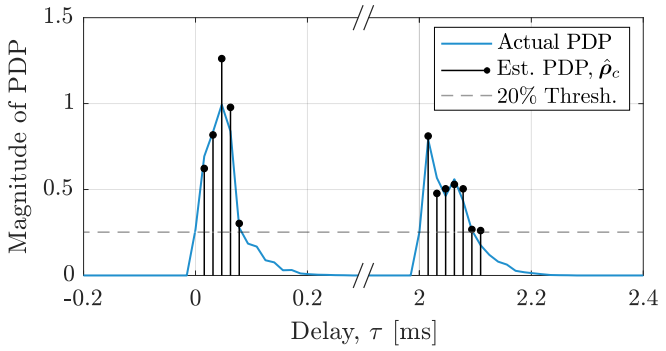

Fig. 3. Comparison of the actual and estimated channel PDPs, $\boldsymbol{\rho}_c$ and $\hat{\boldsymbol{\rho}}_c$, respectively, in a channel with a Doppler spread of 4 Hz. The estimates are generated from a signal received at 0 dB SNR from a total of $N_\mathrm{p} = 64$ pilot symbols. For clarity, the x-axis is zoomed to the regions containing nonzero channel information.

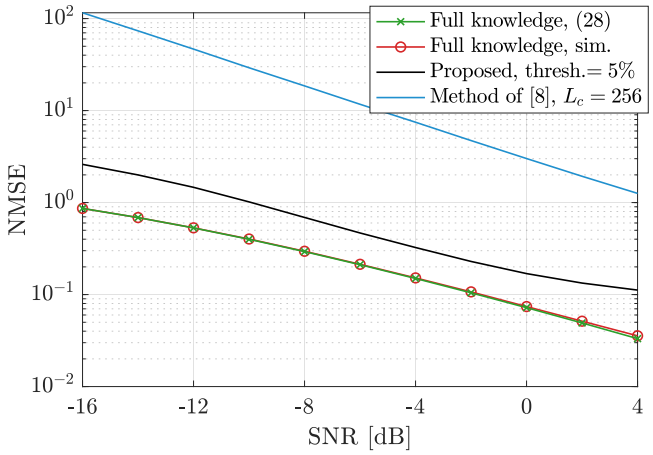

Fig. 4. NMSE comparison of the proposed estimator, the method of [8], and an estimator with perfect knowledge of the channel information when applied to a single received preamble sequence.

B. Channel Estimator

We now proceed to evaluate the performance of the PDP estimator when used in tandem with the channel estimator of Section III-B. The error of the proposed two-stage estimator is quantified as $\boldsymbol{\xi} = \mathbf{c} - \hat{\mathbf{c}}$, where $\mathbf{c}$ is the actual channel response and $\hat{\mathbf{c}}$ is the estimated response. For the simulated results, we measure the normalized mean-squared error (NMSE) as

$$\mathrm{NMSE} = \frac{\boldsymbol{\xi}^\mathrm{H}\boldsymbol{\xi}}{\mathbf{c}^\mathrm{H}\mathbf{c}}. \tag{27}$$

Taking the expectation of (27) provides a theoretical performance of the MMSE estimator from (23). Following [10] and assuming the noise is AWGN, we obtain

$$\mathrm{NMSE}_\mathrm{theory} = \frac{\mathrm{tr}\left[\left(\boldsymbol{\Sigma}_{c_\mathrm{p}c_\mathrm{p}}^{-1} + \frac{1}{\sigma_v^2}\boldsymbol{\mathcal{F}}_\mathrm{p}^\mathrm{H}\mathbf{G}_\mathrm{f}^*\mathbf{G}_\mathrm{f}\mathbf{Z}_\mathrm{f}^*\mathbf{Z}_\mathrm{f}\boldsymbol{\mathcal{F}}_\mathrm{p}\right)^{-1}\right]}{\mathbb{E}[\mathbf{c}^\mathrm{H}\mathbf{c}]}, \tag{28}$$

where σ_v^2 is the noise variance and $\mathrm{tr}[\cdot]$ denotes trace of. Here, the $\boldsymbol{\mathcal{F}}_\mathrm{p}$ matrices contain the columns corresponding to each nonzero tap position present in the actual channel response. We relate the noise variance to the SNR as

$$\mathrm{SNR} = \frac{\sigma_{x_c}^2}{\sigma_v^2}, \tag{29}$$

where $\sigma_{x_c}^2 = \mathbb{E}[|x_c(t)|^2]$ is power of the signal contribution at the receiver input.

In Fig. 4, we compare the results of the proposed estimator to an alternative channel estimation approach from [8], to the performance when the estimator is given perfect knowledge of the channel PDP, and to the theoretical bound of (28).

For the proposed estimator, in this case, the OMP algorithm terminates when either the magnitude of the tap estimate falls below 5% of the maximum tap or when the number of nonzero taps reaches 100. At a termination threshold of 5%, many taps of $\hat{\boldsymbol{\rho}}_c$ may be either missed or falsely selected, resulting in an elevated error compared to the theoretical bound.

For the approach taken in [8], the estimator does not account for the sparsity of the channel response. Instead, the channel response is assumed to be limited to a span of L_c samples. In this case, we select $L_c = 256$ which corresponds to a channel duration of 4 ms. For this estimator, the PDP estimate is neglected and the MMSE estimator of (23) is used where the pruned DFT matrix and channel vectors, $\boldsymbol{\mathcal{F}}_\mathrm{p}$ and $\mathbf{c}_\mathrm{p}$, respectively, correspond to the first L_c taps of the channel vector. Moreover, since the PDP of the channel is unknown, the channel tap covariance matrix is $\boldsymbol{\Sigma}_{c_\mathrm{p}c_\mathrm{p}} = \mathbf{I}$.

Lastly, in the case where the channel estimate is obtained with perfect (i.e., full) PDP knowledge, the NMSE performance aligns with (28) at low SNRs, but appears to diverge with increasing SNR. The difference between these curves is a constant error offset resulting from the 4 Hz of Doppler, leading to a slight variation in the channel response over the duration of the preamble.

C. Time varying channel estimate

Here, we demonstrate the tracking performance of the estimator. Following the procedure detailed in Section III-B, for each inserted pilot symbol, a channel estimate is generated and subsequently smoothed using a filter whose impulse response has a Gaussian shape tuned for a Doppler spread of 10 Hz.

Fig. 5 compares the estimated and actual magnitudes of a single channel path as it varies with time for a signal received at 0 dB SNR. There are two observations to be made from this figure: first, the channel estimate remains accurate even when the magnitude of the channel path is low. Second, despite being smoothed by a filter whose passband was much wider than the Doppler spread of the channel, the estimated magnitudes remain close to the actual channel response.

V. Conclusion

In this paper, we developed a method for estimating sparse and doubly-dispersive channels. This method comprises two stages, the first of which uses known pilot symbols inserted throughout the packet to estimate the power-delay profile (PDP) of the channel. In the second stage, the PDP estimate is used to reduce the number of parameters in the channel estimator, reducing the complexity of channel acquisition and tracking while also reducing the error in the resulting estimate.

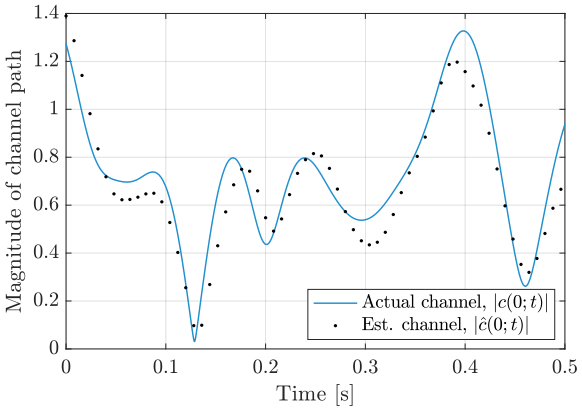

Fig. 5. Actual and estimated channel response magnitudes at delay $\tau = 0$ over the payload section of the packet at the pilot symbol positions. The channel Doppler is 4 Hz and the signal is received at SNR $= 0$ dB.

A case study of the proposed estimator was compared with an existing estimation method presented in [8]. The results show a significant improvement over this existing method in the low-SNR and doubly-dispersive operating environments typical for spread-spectrum systems.

References

[1] X. Yang, S. Houcke, C. Laot, and H. Wang, "Soft decision feedback equalizer for channels with low SNR in underwater acoustic communications," in *2013 MTS/IEEE OCEANS - Bergen*, (Bergen), p. 1–5, IEEE, Jun 2013.

[2] E. Johnson, E. Koski, W. Furman, M. Jorgenson, and J. Nieto, *Third-Generation and Wideband HF Radio Communications*. Artech House, 2013.

[3] H. Minn and V. Bhargava, "An investigation into time-domain approach for OFDM channel estimation," *IEEE Transactions on Broadcasting*, vol. 46, p. 240–248, Dec 2000.

[4] S. Cotter and B. Rao, "Sparse channel estimation via matching pursuit with application to equalization," *IEEE Transactions on Communications*, vol. 50, p. 374–377, Mar 2002.

[5] S. Cotter and B. Rao, "The adaptive matching pursuit algorithm for estimation and equalization of sparse time-varying channels," in *Conference Record of the Thirty-Fourth Asilomar Conference on Signals, Systems and Computers (Cat. No.00CH37154)*, vol. 2, (Pacific Grove, CA, USA), p. 1772–1776, IEEE, 2000.

[6] C. R. Berger, Z. Wang, J. Huang, and S. Zhou, "Application of compressive sensing to sparse channel estimation," *IEEE Communications Magazine*, vol. 48, p. 164–174, Nov 2010.

[7] J.-J. Van De Beek, O. Edfors, M. Sandell, S. Wilson, and P. Borjesson, "On channel estimation in OFDM systems," in *1995 IEEE 45th Vehicular Technology Conference. Countdown to the Wireless Twenty-First Century*, vol. 2, (Chicago, IL, USA), p. 815–819, IEEE, 1995.

[8] J. Driggs, T. Sibbett, H. Moradi, and B. Farhang-Boroujeny, "Channel estimation for filter bank multicarrier systems in low SNR environments," in *2017 IEEE International Conference on Communications (ICC)*, (Paris, France), p. 1–7, IEEE, May 2017.

[9] G. Taubock and F. Hlawatsch, "A compressed sensing technique for OFDM channel estimation in mobile environments: Exploiting channel sparsity for reducing pilots," in *2008 IEEE International Conference on Acoustics, Speech and Signal Processing*, (Las Vegas, NV, USA), p. 2885–2888, IEEE, Mar 2008.

[10] S. M. Kay, *Fundamentals of statistical signal processing*, vol. 1 of *Prentice Hall signal processing series*. Englewood Cliffs, N.J: Prentice-Hall PTR, 1993.

[11] M. Raghavendra and K. Giridhar, "Improving channel estimation in OFDM systems for sparse multipath channels," *IEEE Signal Processing Letters*, vol. 12, p. 52–55, Jan 2005.

[12] J. Oliver, R. Aravind, and K. Prabhu, "Sparse channel estimation in OFDM systems by threshold-based pruning," *Electronics Letters*, vol. 44, no. 13, p. 830, 2008.

[13] T. E. Bogale, X. Wang, and L. B. Le, "Dominant CIR tap identification for OFDM channels: Adaptive bootstrapping approach," in *ICC 2019 - 2019 IEEE International Conference on Communications (ICC)*, pp. 1–7, 2019.

[14] L. Silva and J. Gomes, "Sparse channel estimation and equalization for underwater filtered multitone," in *OCEANS 2015 - Genova*, (Genova, Italy), p. 1–8, IEEE, May 2015.

[15] J. Cavers, "An analysis of pilot symbol assisted modulation for Rayleigh fading channels (mobile radio)," *IEEE Transactions on Vehicular Technology*, vol. 40, p. 686–693, Nov 1991.

[16] D. Wasden, H. Moradi, and B. Farhang-Boroujeny, "Design and implementation of an underlay control channel for cognitive radios," *IEEE Journal on Selected Areas in Communications*, vol. 30, p. 1875–1889, Oct 2012.

[17] K.-C. Hung and D. Lin, "Pilot-based LMMSE channel estimation for OFDM systems with power–delay profile approximation," *IEEE Transactions on Vehicular Technology*, vol. 59, p. 150–159, Jan 2010.

[18] A. Khlifi and R. Bouallegue, "A very low complexity LMMSE channel estimation technique for OFDM systems," in *2015 IEEE 81st Vehicular Technology Conference (VTC Spring)*, (Glasgow, United Kingdom), p. 1–5, IEEE, May 2015.

[19] T. Yucek and H. Arslan, "Time dispersion and delay spread estimation for adaptive OFDM systems," *IEEE Transactions on Vehicular Technology*, vol. 57, p. 1715–1722, May 2008.

[20] D. Tse and P. Viswanath, *Fundamentals of Wireless Communications*. Cambridge University Press, 1 ed., 2005.

[21] J. G. Proakis and M. Salehi, *Digital communications*. Boston: McGraw-Hill, 5th ed ed., 2008.

[22] J. G. Proakis and D. G. Manolakis, *Digital signal processing*. Upper Saddle River, N.J: Pearson Prentice Hall, 4th ed ed., 2007.

[23] S. Theodoridis, *Machine Learning: A Bayesian and Optimization Perspective*. Academic Press, 1 ed., 2015.

[24] Y. Pati, R. Rezaiifar, and P. Krishnaprasad, "Orthogonal matching pursuit: recursive function approximation with applications to wavelet decomposition," in *Proceedings of 27th Asilomar Conference on Signals, Systems and Computers*, (Pacific Grove, CA, USA), p. 40–44, IEEE Comput. Soc. Press, 1993.

[25] L. Rebollo-Neira and D. Lowe, "Optimized orthogonal matching pursuit approach," *IEEE Signal Processing Letters*, vol. 9, p. 137–140, Apr 2002.

[26] D. Haab, H. Moradi, and B. Farhang-Boroujeny, "Spread spectrum symbol detection with blind interference suppression in FBMC-SS," *IEEE Open Journal of the Communications Society*, vol. 2, p. 1630–1646, Jul 2021.

[27] R. M. Gray, "Toeplitz and circulant matrices: A review," *Foundations and Trends® in Communications and Information Theory*, vol. 2, no. 3, p. 155–239, 2005.

[28] B. L. Sturm and M. G. Christensen, "Comparison of orthogonal matching pursuit implementations," in *2012 Proceedings of the 20th European Signal Processing Conference (EUSIPCO)*, pp. 220–224, 2012.

[29] B. Hunt, D. Haab, T. Sego, T. Holschuh, H. Moradi, and B. Farhang-Boroujeny, "Examining the performance of MIL-STD-188-110D waveform 0 against FBMC-SS in skywave HF channels," *IEEE Transactions of Vehicular Technology*, 2022.

[30] S. Laraway, H. Moradi, and B. Farhang-Boroujeny, "HF band filter bank multi-carrier spread spectrum," in *MILCOM 2015 - 2015 IEEE Military Communications Conference*, (Tampa, FL), Oct 2015.

[31] D. B. Haab, T. C. Sego, T. V. Holschuh, H. Moradi, and B. Farhang-Boroujeny, "Multicode signaling in a filter bank multicarrier spread spectrum system and its application to HF communications," *IEEE Open Journal of the Communications Society*, vol. 4, p. 442–455, 2023.

[32] J. Mastrangelo, J. Lemmon, L. Vogler, J. Hoffmeyer, L. Pratt, and C. Behm, "A new wideband high frequency channel simulation system," *IEEE Transactions on Communications*, vol. 45, p. 26–34, Jan 1997.